



LAWRENCE
LIVERMORE
NATIONAL
LABORATORY

Application of fall-line mix models to understand degraded yield

L. Welser-Sherrill, J. H. Cooley, D. A. Haynes, D.
C. Wilson, M. E. Sherrill, R. C. Mancini, R.
Tommasini

March 18, 2008

Physics of Plasmas

Disclaimer

This document was prepared as an account of work sponsored by an agency of the United States government. Neither the United States government nor Lawrence Livermore National Security, LLC, nor any of their employees makes any warranty, expressed or implied, or assumes any legal liability or responsibility for the accuracy, completeness, or usefulness of any information, apparatus, product, or process disclosed, or represents that its use would not infringe privately owned rights. Reference herein to any specific commercial product, process, or service by trade name, trademark, manufacturer, or otherwise does not necessarily constitute or imply its endorsement, recommendation, or favoring by the United States government or Lawrence Livermore National Security, LLC. The views and opinions of authors expressed herein do not necessarily state or reflect those of the United States government or Lawrence Livermore National Security, LLC, and shall not be used for advertising or product endorsement purposes.

Application of fall-line mix models to understand degraded yield

L. Welsler-Sherrill,¹ J.H. Cooley,¹ D.A. Haynes,¹ D.C. Wilson,¹ M.E. Sherrill,¹ R.C. Mancini,² and R. Tommasini³

¹*Los Alamos National Laboratory, Los Alamos, New Mexico, 87545*

²*Department of Physics, University of Nevada, Reno, Nevada, 89557*

³*Lawrence Livermore National Laboratory, Livermore, California, 94550*

(Dated: January 3, 2008)

Mixing between fuel and shell material is an important topic in the inertial confinement fusion community, and is commonly accepted as the primary mechanism for neutron yield degradation. Typically, radiation hydrodynamic simulations that lack mixing (clean simulations) tend to considerably overestimate the neutron yield. We present here a series of yield calculations based on a variety of fall-line inspired mix models. The results are compared to a series of OMEGA experiments which provide total neutron yields and time-dependent yield rates.

PACS numbers: 52.57.-z, 47.20.Ma, 47.51.+a

I. INTRODUCTION

An important objective of inertial confinement fusion (ICF) is to determine a methodology for evaluating implosion quality. In ICF, a capsule filled with fuel is imploded either directly, by the application of laser beams onto its surface, or indirectly, in a soft x-ray radiation bath [1]. The resulting implosion is confined by the inertia of the fuel mass, and fusion reactions take place in the core [2].

One issue that has broadly affected ICF is the understanding of mix. When a capsule implodes, some of the hot fuel material (usually deuterium and/or tritium) mixes with the cooler material of the outer shell (plastic and glass are common). This fuel-shell mix quenches the fusion reactions and therefore the neutron yield. The control and mitigation of mix is an important goal for achieving ignition, which occurs when the plasma is sustained by fusion reactions without energy input from external sources [1].

Radiation hydrodynamics simulations are a valuable tool for designing and understanding ICF implosions. Generally, simulations of specific experiments are reasonably good at predicting the temperatures, densities, pressures, and other physical characteristics of the implosions. However, when performing a clean simulation, which by definition does not incorporate any mixing between fuel and shell materials, the neutron yield is consistently over-predicted as compared to experiment.

A metric called the yield-over-clean (YoC), which is the ratio of the experimental primary neutron yield to the calculated clean yield with no mix, represents a standard measurement of implosion performance [3–6]. A small value for the YoC therefore implies severe yield degradation, while a YoC approaching unity implies that the yield is not degraded as compared to the clean calculation.

Amendt *et al*, in their study of double-shell capsules, approached this problem by optimizing the fall-line behavior, which tends to minimize mix [3, 4]. The fall-line is traditionally defined as the straight-line trajec-

tory drawn tangent to the fuel-shell interface at the point when the interface begins to decelerate. In essence, the fall-line represents the peak shell velocity in a hydrodynamic sense, as well as an upper bound for contamination of the fuel. The mixed fuel-shell material should remain behind the fall-line, because by causality it cannot move faster than the peak velocity. Amendt *et al* [3] used this idea to design experiments which had high YoC and thus minimized the amount of mix.

In the work presented here, we use the concepts of the fall-line to apply a number of methods that calculate the mix-degraded yield by post-processing hydrodynamic simulations. We discuss the applicability of different modifications of the fall-line as compared to the traditional fall-line approach. We also evaluate an interface penetration fraction model developed by Amendt *et al* [4]. Finally, we apply Haan's saturation model [7] to our test problems and investigate the corresponding yield degradation behavior.

We focus on a particular set of experiments for which detailed hydro simulations were performed. The simulations were calibrated with data from the experiments, and a post-processing procedure was developed to implement the mix models. By comparing the experimental yield data to results of the mix models, we can validate and judge the applicability of each model.

II. EXPERIMENTS

The methods described here were tested with a set of direct-drive experiments performed at the Laboratory for Laser Energetics' OMEGA laser [8]. The targets were plastic capsules with outer radii of $435.5 \pm 1.4 \mu\text{m}$, and were filled with 20 atm of D_2 and 0.072 atm of Ar. These implosions use plastic shells and deuterium gas to simulate conditions during the deceleration phase. Of the eight experimental shots reported here, five had $\sim 26 \mu\text{m}$ thick shells, two had $\sim 19 \mu\text{m}$ shells, and one had an $\sim 32 \mu\text{m}$ shell. A 1-ns square laser pulse with $\sim 23 \text{kJ}$ of energy irradiated the target in each case.

Time-dependent neutron yield data were recorded with

TABLE I: List of experiments, including shell thicknesses and total neutron yields from the nTOF detector. Shot sequence A represents the $\sim 26 \mu\text{m}$ shells, sequence B represents the thinner $\sim 19 \mu\text{m}$ shells, and sequence C is the thicker $\sim 32 \mu\text{m}$ shell.

Shot	Shell Thickness	Neutron Yield
1A	25.8 μm	2.87×10^{10} ($\pm 1.3\%$)
2A	25.6 μm	3.16×10^{10} ($\pm 1.2\%$)
3A	25.8 μm	2.89×10^{10} ($\pm 1.3\%$)
4A	25.6 μm	2.84×10^{10} ($\pm 1.3\%$)
5A	25.7 μm	2.94×10^{10} ($\pm 1.3\%$)
1B	19.3 μm	1.35×10^{11} ($\pm 0.6\%$)
2B	19.3 μm	1.31×10^{11} ($\pm 0.6\%$)
1C	32.2 μm	5.83×10^9 ($\pm 2.8\%$)

the Neutron Temporal Diagnostic (NTD) [9], which in this case measured the number of 2.45 MeV neutrons produced in the $D+D \rightarrow n + {}^3\text{He}$ reaction as a function of time. As an additional diagnostic, the total number of neutrons produced was provided by the Neutron Time-of-Flight (nTOF) [10] instrument. Both of these measurements were used to compare directly to the results of the theoretical mix models studied. Table I lists the eight experimental shots and their corresponding shell thicknesses and total yields.

III. THEORETICAL MODELING

The simulations used in this work were performed with the 1-D Lagrangian radiation hydrodynamics code HELIOS-CR [11, 12], which calculates in-line Non-Local Thermodynamic Equilibrium (NLTE) collisional-radiative atomic kinetics for every time step and every spatial zone in the simulation.

In comparing theory to experiment, a collection of simulations was calibrated to conform as closely as possible to the actual conditions of each of the eight experimental shots described above. The beam-averaged laser pulse power spectrum as a function of time was used for every individual shot, and the experimentally measured shell thicknesses from Table I were also employed. In addition, the flux limiter was modified until the experimental bang time matched the clean yield bang time for each case.

To study how mix degrades neutron yield, the hydrodynamic simulations were post-processed with FLAME¹ (Fall-Line Analysis Mix Evaluator), an interactive graphical user interface tool documented in Ref. [13]. The detailed figures in this paper represent the results of analyzing the hydro simulations representing one experiment

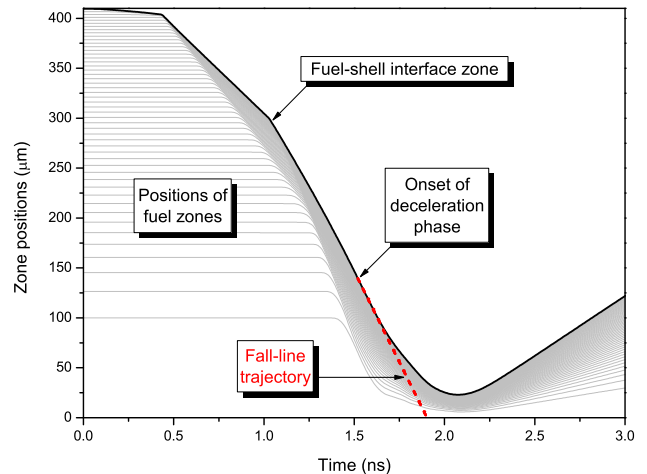


FIG. 1: (Color online) Position of the fuel-shell interface zone (thick black) as a function of time, and the corresponding traditional fall-line trajectory (red dots). The positions of all fuel zones are also shown (thin grey). The fall-line intersects each zone at a slightly different time. In this implementation of the traditional fall-line model, the yields are fully dudded behind the fall-line. (FLAME analysis of Shot 5A from Table I.)

(Shot 5A in Table I). The same procedure was also followed with the other seven shots, and the resulting yields will be discussed and shown in Section V. In the following subsections, we describe the procedures and results of implementing four different mix models with FLAME.

A. Fall-Line Mix Model

We begin with the fall-line itself. Figure 1 shows the zone position for the fuel-shell interface as a function of time, and the traditional definition of the fall-line, whose slope is set at the onset of the deceleration phase (the time of peak velocity). The fall-line continues until it encounters $r = 0$. Physically, the fall-line represents the maximum theoretical rate of shell contamination of the fuel, since it continues the trajectory of the fuel-shell interface when it is moving at its peak velocity.

The positions of every zone in the gas are plotted along with the fall-line. Figure 1 shows how the fall-line intersects each zone at a slightly different time. These times, which are referred to as t_{zone} , are the times when yield degradation, or dudding, begins for each zone.

The yield degradation is performed independently for every zone. In the simplest form, we can naively assume complete dudding in the next time step following each t_{zone} ; in other words, the zone's yield drops to zero in the next time step. This completely dudded fall-line model (which will be referred to here as the traditional fall-line model) is shown in Figure 2(a), along with other mix models which will be discussed in the subsequent sections. In Figure 3(a), the black lines show the clean yields

¹ FLAME is available with complete documentation by contacting Leslie Welser-Sherrill at lwelser@lanl.gov.

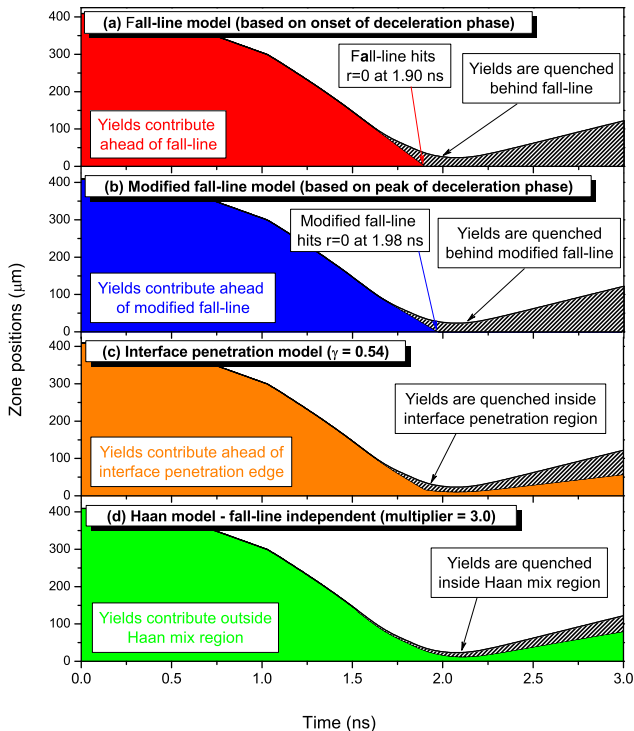


FIG. 2: (Color online) Spatial and temporal regions where yield contributes, according to the four mix models discussed here, are shown in solid colors. Regions where yield degradation occurs are shown in striped black and white. (a) Traditional fall-line mix model, where the slope is set at the onset of the deceleration phase. (b) Modified fall-line mix model based on a fall-line which sets the slope at the peak of the deceleration phase. (c) Interface penetration fraction model representing a total yield that matches the experimental yield ($\gamma = 0.54$). (d) Independent mix model based on Haan’s saturation model (multiplier = 3.0). (FLAME analysis of Shot 5A from Table I.)

for every hydro zone, while the colored circles represent only the yields that contribute in the fall-line model. Note that the innermost zone (with a position closest to $r = 0$) has the largest yield rate, while the outermost fuel zone (next to the interface) has the smallest yield rate. This means that the traditional fall-line analysis eventually duds the yield in all zones, since the fall-line region hits $r = 0$ at a time when neutrons are still being produced, according to the clean simulation.

Though the traditional fall-line model represents the fastest way for the shell material to contaminate the fuel and thus induce yield degradation, it is not likely that the in-fall of shell material would be so violent. We therefore also studied an alternative approach to the traditional fall-line model in which the yield is quenched only partially (not shown graphically here) by using a longer transient yield degradation after the fall-line intersects each zone. This is a free parameter in the analysis, and can be used to match experimental data.

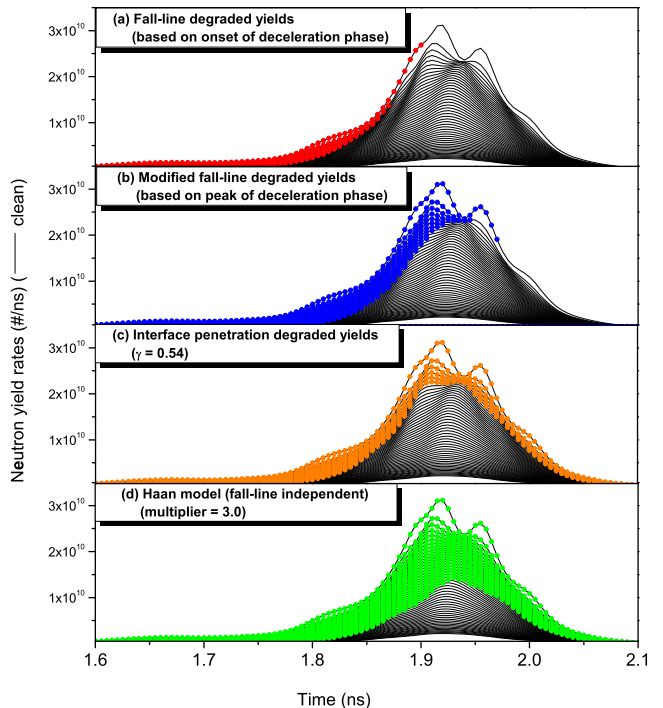


FIG. 3: (Color online) Clean yield rates predicted by HELIOS for all fuel zones (black solid) and degraded yields calculated by the four mix models discussed here. Contributing yields are shown in colored circles, while the remaining regions are duded. (a) Traditional fall-line mix model, where the slope is set at the onset of the deceleration phase. (b) Modified fall-line mix model based on a fall-line which sets the slope at the peak of the deceleration phase. (c) Interface penetration fraction model representing a total yield that matches the experimental yield ($\gamma = 0.54$). (d) Independent mix model based on Haan’s saturation model (multiplier = 3.0). (FLAME analysis of Shot 5A from Table I.)

B. Modified Fall-Line Mix Model

As will be demonstrated in Section IV, applying the traditional fall-line approach results in an exaggerated yield degradation which does not match the experimental data. We therefore implement two modifications to the traditional fall-line described above.

The first approach to modify the fall-line stems from a simple model designed to match the experimental data with the help of a free parameter. The slope of the fall-line was defined previously as the velocity of the free-falling shell material. A parameter-based modified fall-line is introduced to relax this slope, and effectively decreases the yield degradation modeled in the traditional fall-line case. This method assumes simply that the shell material is moving at a slower velocity than the free-falling shell represented by the traditional fall-line. This version of the modified fall-line also starts its trajectory at the onset of the deceleration phase, but it intersects

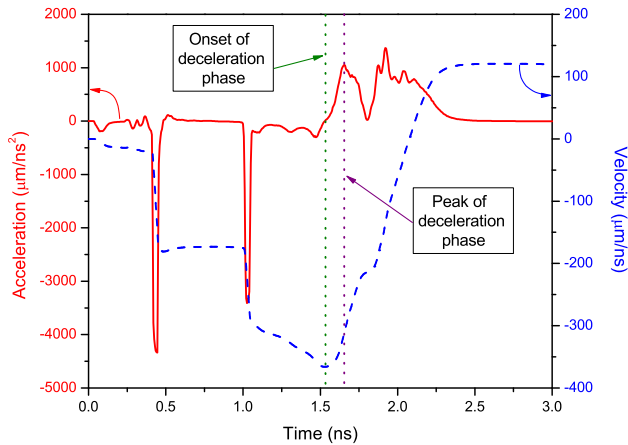


FIG. 4: (Color online) Acceleration and velocity profiles highlighting the onset and peak of the deceleration phase (based on HELIOS-CR simulation of Shot 5A from Table I.)

the $r = 0$ axis (signifying complete mixing of the core) at a later time. We define a parameter Δt as the difference between the time when the traditional fall-line and the modified fall-line hit $r = 0$. With this approach, the free parameter Δt (and the associated modified fall-line velocity) can be used to control the yield-dudding effect. We have performed a sensitivity study for the value of Δt over the range of eight experimental shots described here. The average value for Δt was 72 ps, with a standard deviation of 14 ps, and it was not particularly sensitive to the different shell thicknesses employed. Although this simple model allows us to consistently match the experimental yield with similar parameters, it does not provide a sound physical interpretation for the parameter associated with the fall-line relaxation.

We therefore implemented another more physical approach to modify the fall-line. The traditional concept of the fall-line is based on defining the *onset* of the deceleration phase. However, since the application of this technique results in severe yield degradation, we have investigated a number of other constructions for modified fall-lines. This study demonstrated that a modified fall-line based on the *peak* of the deceleration phase rather than the onset resulted in a yield degradation closely matching the experimental yields. Figure 4 shows a representative case for the acceleration and velocity profiles, with the onset and peak of the deceleration phase labeled. Recall that the traditional fall-line begins at the time of peak velocity, which is a singular event corresponding to the onset of the deceleration phase. When we set a modified fall-line based on the peak of the deceleration phase (also a singular event), there is some uncertainty in the determination of the slope due to the more nonlinear nature of the fuel-shell interface at this later time. We use this uncertainty to define the error bars in the final degraded yield. Figures 2(b) and 3(b) demonstrate the results of this method.

C. Interface Penetration Fraction Mix Model

The spatial evolution of the mixing region as a function of time can be modeled in terms of a constant (time-independent) fraction of the distance between the interface and the fall-line. This approach was described by Amendt *et al* in Ref. [4].

In our implementation of the interface penetration model, the penetration fraction γ can be explicitly chosen to produce a degraded theoretical yield that matches the experimental yield. Figures 2(c) and 3(c) show an example of implementing an interface penetration fraction of 0.54, which translates into a mixing region that is defined to reach 54% of the distance between the interface and the fall-line (or the $r=0$ axis if the fall-line has already intersected it). In the case discussed here, this value for γ produces a degraded yield that matches experiment.

A sensitivity study over the range of experimental shots showed very little dependence on the shell thickness. The average value for γ was 0.54, with a standard deviation of 0.03. This uncertainty in the value of γ across all eight shots studied here was used to set the error bars for the model.

D. Haan Mix Model

For comparison here, we present the results of a time-dependent Haan mix model, which is based on the techniques presented in Ref. [14]. Hydro simulations were first post-processed according to the prescription set forth by Haan in Ref. [7]. The Haan saturation model calculates the mix width due to Rayleigh-Taylor instability growth, which occurs when a lower-density fluid (the fuel) pushes against a higher-density fluid (the shell) [15, 16]. Haan's model infers mix width characteristics based on estimating the growth of multi-mode perturbations on the fuel-shell interface. For these direct-drive experiments, we use perturbation spectra based on the target surface roughness, the laser beam power imbalance, and the laser imprint [17, 18].

This particular implementation of the Haan model calculates the time-dependent growth of the mixing region [13]. The mix width itself is broken down into the bubble and spike widths, which sum to the total mix width. In applying the Haan model to the fuel-shell interface, we use only the spike width, which represents the spatial extent of heavier shell material into the lighter gas. Figure 2(d) shows that in this case, the mix region defined by Haan's model is significantly smaller than the mix regions found in the fall-line based models. Therefore, as is demonstrated in Figure 3(d), the yields in the hydro zones closest to the center of the capsule never experience degradation. Since the yields in these zones are the highest, the resulting total yield is closer to the clean calculation than the models which use the fall-line to describe mix.

In other work, we have previously studied the effect

that a constant multiplier on the initial perturbations has on the mix width [14]. We found that in those cases, which were indirect-drive experiments, a multiplier of 3.0 resulted in a mix width which matched the experimentally-derived mix width. We use the range of multipliers from 1.0 (the nominal Haan model) to 3.0 (the experimentally calibrated value) to determine an uncertainty level for this application of the Haan model. It is interesting to note that the application of a multiplier of 3.0 on the initial perturbations does not drastically affect the yield degradation or bring the Haan yield down to the experimental level in all cases. This is due to the fact that a larger Haan mix width still does not dud the yield in the innermost zones of the problem, where the yield is highest. The behavior of the Haan mixing region is such that the shell material never reaches the center, and thus full contamination never occurs.

IV. COMPARISON OF YIELD DEGRADATION EFFECTS AND EXPERIMENTAL DATA

As described above, four mix models were used to calculate the degraded yield rates for all zones. The yields from all zones were then simply added to compile a total integrated yield curve for each mix model. In Figure 5, we demonstrate the effects of mix-degraded yield by plotting the total clean yield rate along with the integrated yield rates from each of the four models as a function of time.

The total degraded yield rates were compared with the experimental yield rate as a function of time, which in this case was recorded with the Neutron Temporal Diagnostic (NTD). The experimental data, however, was given in terms of CCD counts, and therefore was normalized so that the area under the curve matched the experimental integrated yield given by the neutron time-of-flight (NTOF) diagnostic. In order to compare the theoretical yield curves to that of the experiment, the degraded yield rates shown in Figure 5 were convolved with a 40-ps Gaussian, the instrumental response of the NTD detector [9].

It is clear from Figure 5 that the experimental yield rate most closely matches that of the interface penetration model. This result substantiates the conclusion of Amendt *et al* [4], which described the theoretical basis for representing the spatial evolution of fuel-shell mix in terms of a constant fraction of the distance between the interface and the fall-line. Analyses of the remainder of the experimental shots from Table I demonstrate that in all cases, the experimental yield traces are best described by the interface penetration model.

The theoretical yield rate curves of Figure 5, representing the number of neutrons produced per nanosecond, were integrated over the simulation time to calculate the total neutron yield. Using the same methods discussed above, the set of simulations representing the eight experimental cases defined in Table I were also post-processed.

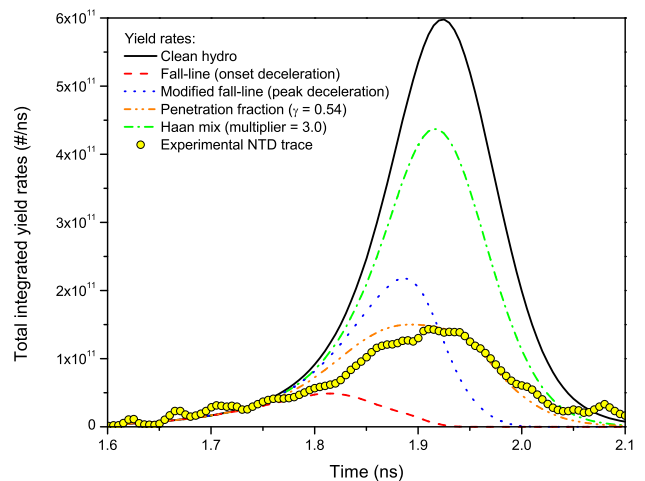


FIG. 5: (Color online) A comparison of the total clean yield rate as predicted by the HELIOS simulation, and degraded yield rates from the traditional fall-line model, the modified fall-line model based on the peak of the deceleration phase, the interface penetration fraction model ($\gamma = 0.54$), and the Haan saturation model (multiplier = 3.0). (FLAME analysis of Shot 5A from Table I.)

By investigating a number of cases, we were able to accumulate better statistics on the performance of the mix models discussed.

The total clean yields predicted by the HELIOS simulations, as well as the different flavors of degraded total yields, are plotted in Figure 6 along with the experimental values for the total neutron yields. The experimental uncertainties are within the symbol size. The traditional fall-line gives an estimate of the upper bound expected for mixing. For the modified fall-line model, we used the uncertainty in the slope starting from the peak of the deceleration phase to set the error bars. In the case of the interface penetration model, which used a flexible parameter to match the experimental yields, the uncertainty bars represent the spread in yield derived by recalculating the degraded yields using the spread in the interface penetration parameter across all simulations. Finally, for the Haan saturation model, the uncertainties represent the spread in yield resulting from the use of a range of multipliers on the initial perturbation amplitudes.

As expected, the yield degradation of the traditional fall-line model is the most extreme. The experimental yields lie roughly halfway between the fall-line yields and the clean yields on a log scale.

The results of the modified fall-line model, which uses the peak of the deceleration phase to set the fall-line, demonstrate that the overall yield matches the experimental values very well for all but the thick shell case. Interestingly, as seen in Figure 5, the yield rate from the modified fall-line technique does not provide the best match to the experimental yield rate.

As was intended in this implementation of the inter-

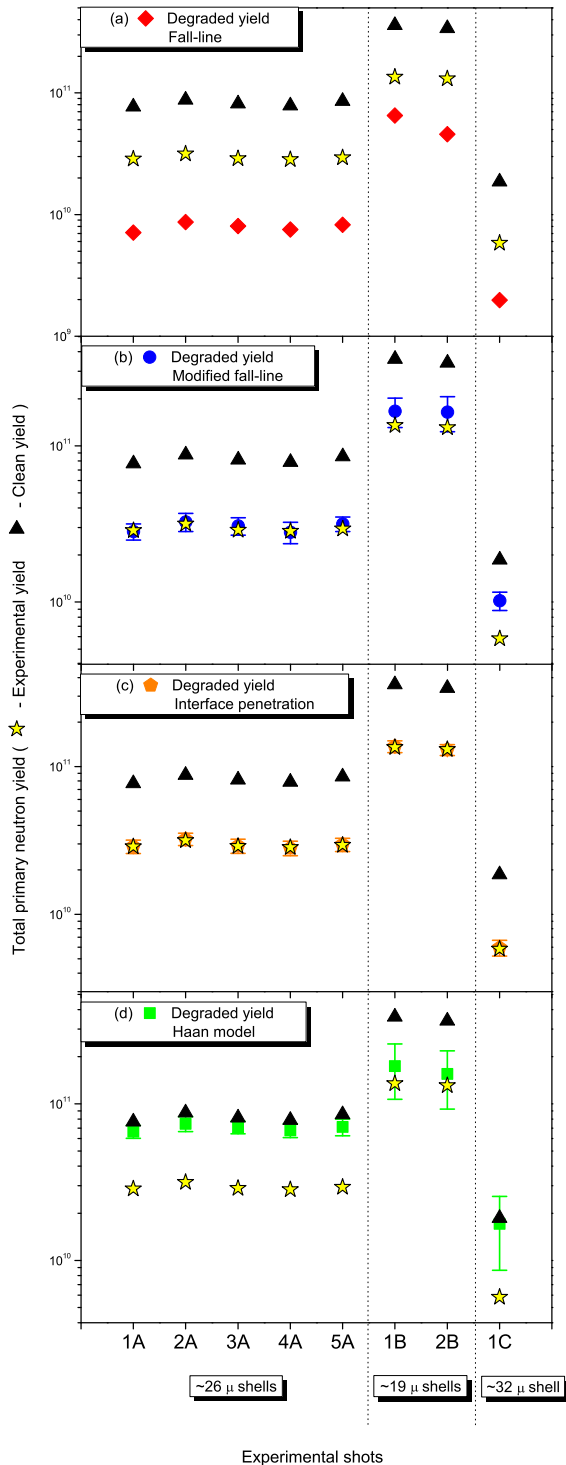


FIG. 6: (Color online) Comparison between experimental yields (yellow stars, experimental uncertainties within symbol size), the clean yields predicted by HELIOS (black triangles), and the degraded yields based on (a) the traditional fall-line analysis (red diamonds), (b) the modified fall-line analysis (blue circles), (c) the interface penetration fraction model (orange pentagons), and (d) the Haan mix model (green squares). The shell thickness corresponding to each experiment (and thus each simulation) is noted at the bottom.

face penetration model, the error bars of the associated yields are within the range of the experimental yields in all cases. We note that although a free parameter was used to guide the total yield result, this technique provided excellent agreement between the calculated yield rate curve and the experimental NTD data. An investigation into a physical interpretation for this model that would preclude the use of a free parameter is ongoing.

The results of the Haan model yield degradation are complex. For the mid-range 26 μ m shells, the Haan model inferred relatively small mix widths, corresponding to a low yield degradation and resulting in yields close to clean. This effect was even more obvious in the thick 32 μ m shell case, since the Haan model predicted even lower levels of mix. However, in the case of the thin 19 μ m shells, the Haan model calculates substantially larger mix widths, resulting in yields that are closer to experiment. In fact, this trend was noticed during the design phase of the experimental campaign, when the Haan saturation model was used to investigate the design parameter space for capsules which would result in varying levels of mix. Therefore, it is not surprising that Haan's model results in a more substantial yield degradation for the thin shell targets.

Table II shows the yield-over-clean (YoC) measurements for the experimental data, comparing the clean hydro yields to the experimental yields. The range of 0.3-0.4 for the YoC demonstrates that the clean hydro yields are significantly overestimated. We use a similar concept, called the yield-over-mix (YoM), which represents a comparison between the experimental yields and the calculated degraded yields. Table II presents the YoM measurements for the four yield degradation models discussed here. For the traditional fall-line model, the YoM is greater than one, since this model underestimates the yield. Using a modified fall-line based on the peak of the deceleration phase resulted in YoM values close to one. In the case of the interface penetration fraction model, the YoM measurements are significantly closer to 1.0, repre-

TABLE II: Yield-over-clean (YoC) and yield-over-mix (YoM) measurements for the eight experimental shots. YoM_{FL} is the traditional fall-line model, YoM_{MFL} represents the modified fall-line model, YoM_{PF} is the penetration fraction model, and YoM_{HM} is the Haan mix model. Shot sequence A represents the ~26 μ m shells, sequence B represents the thinner ~19 μ m shells, and sequence C is the thicker ~32 μ m shell.

Shot	YoC	YoM_{FL}	YoM_{MFL}	YoM_{PF}	YoM_{HM}
1A	0.37	4.04	1.02	1.00	0.43
2A	0.36	3.64	0.97	0.98	0.42
3A	0.36	3.59	0.94	0.99	0.41
4A	0.36	3.76	1.01	1.01	0.42
5A	0.34	3.57	0.93	0.99	0.41
1B	0.38	2.07	0.81	0.99	0.78
2B	0.39	2.86	0.80	1.01	0.84
1C	0.31	2.94	0.57	0.98	0.34

senting the fact that we used the adjustable model parameter to match the experimental and degraded yields as closely as possible. The Haan model YoM shows considerable variation with shell thickness, which is consistent with Figure 5 and the above explanation.

V. CONCLUSIONS

We have studied the degradation of yield due to mix by post-processing 1-D hydrodynamic simulations with a series of mix models. Three mix models that rely on fall-line concepts have been applied: a traditional fall-line model, a modified fall-line model, and an interface penetration model. For comparison, we have also investigated yield degradation within a mix region defined by Haan's saturation model.

The results of the theoretical static mix models have been compared to experimental data from a set of direct-drive OMEGA experiments. By analyzing a number of experimental shots, statistics show that the modeling is appropriate in all studied cases. Using the traditional definition of the fall-line, whose slope is set at the onset of the deceleration phase, we found that the yield degradation is considerably overestimated. If we modify the definition of the fall-line to instead set the slope at the

peak of the deceleration phase, we find that the degraded yields and the experimental yields match well. A single parameter in the interface penetration model was used to match the calculated degraded yields with the experimental yields. Interestingly, we found that the value of the parameter γ was consistent over the range of experiments studied, and therefore we can conclude that this parameter is insensitive to shell thickness. The interface penetration model provides the best match to the experimental yield rate trace.

An important application of this work will be to study the fall-line behavior for a variety of ICF experiments using the tools we have developed. The techniques discussed in this paper represent an evolution in the understanding of how mix affects yield in ICF implosions.

Acknowledgments

This work was performed under the auspices of the U.S. DOE/NNSA Campaign 10 at LANL. The authors wish to acknowledge the support of DOE-NLUF grant DE-FG52-2005NA26012, which provided the experimental campaign. We also thank Igor Golovkin and Joseph MacFarlane (Prism Computational Sciences) for their technical assistance with HELIOS.

-
- [1] J. Lindl, *Phys. Plasmas* **2**, 3933 (1995).
 - [2] J. Nuckolls, L. Wood, A. Thiessen, and G. Zimmerman, *Nature* **239**, 129 (1972).
 - [3] P. Amendt, H. Robey, H.-S. Park, R. Tipton, R. Turner, J. Milovich, M. Bono, R. Hibbard, H. Louis, and R. Wallace, *Phys. Rev. Lett.* **94**, 065004 (2005).
 - [4] P. Amendt, J. Colvin, R. Tipton, D. Hinkel, M. Edwards, O. Landen, J. Ramshaw, L. Suter, W. Varnum, and R. Watt, *Phys. Plasmas* **9**, 2221 (2002).
 - [5] R. Chrien, N. Hoffman, J. Colvin, C. Keane, O. Landen, and B. Hammel, *Phys. Plasmas* **5**, 768 (1999).
 - [6] W. Varnum, N. Delamater, S. Evans, P. Gobby, J. Moore, J. Wallace, R. Watt, J. Colvin, R. Turner, V. Glebov, et al., *Phys. Rev. Lett.* **84**, 5153 (2000).
 - [7] S. Haan, *Phys. Rev. A* **39**, 5812 (1989).
 - [8] T. Boehly, D. Brown, R. Craxton, R. Keck, J. Knauer, J. Kelly, T. Kessler, S. Kumpan, S. Loucks, S. Letzring, et al., *Opt. Commun.* **133**, 495 (1997).
 - [9] R. Lerche, D. Phillion, and G. Tietbohl, *Rev. Sci. Instrum.* **66**, 933 (1995).
 - [10] V. Glebov, C. Stoeckl, T. Sangster, S. Roberts, G. Schmid, R. Lerche, and M. Moran, *Rev. Sci. Instrum.* **75**, 3559 (2004).
 - [11] J. MacFarlane, I. Golovkin, and P. Woodruff, *J. Quant. Spectrosc. Radiat. Transfer* **99**, 381 (2005).
 - [12] J. MacFarlane, I. Golovkin, R. Mancini, L. Welser, J. Bailey, J. Koch, T. Mehlhorn, G. Rochau, P. Wang, and P. Woodruff, *Phys. Rev. E* **72**, 066403 (2005).
 - [13] L. Welser-Sherrill, J. Cooley, and D. Wilson, *Comp. Phys. Comm.* **submitted for publication** (2007).
 - [14] L. Welser-Sherrill, R. Mancini, D. Haynes, S. Haan, J. Koch, N. Izumi, R. Tommasini, I. Golovkin, J. MacFarlane, J. Delettrez, et al., *Phys. Plasmas* **14**, 072705 (2007).
 - [15] L. Rayleigh, *Scientific Papers*, vol. II (Cambridge University Press, 1900).
 - [16] G. Taylor, *Proc. R. Soc. London* **201**, 192 (1950).
 - [17] P. Radha, T. Collins, J. Delettrez, Y. Elbaz, R. Epstein, V. Glebov, V. Goncharov, R. Keck, J. Knauer, J. Marozas, et al., *Phys. Plasmas* **12**, 056307 (2005).
 - [18] P. Radha, V. Goncharov, T. Collins, J. Delettrez, Y. Elbaz, V. Glebov, R. Keck, D. Keller, J. Knauer, J. Marozas, et al., *Phys. Plasmas* **12**, 032702 (2005).

This work performed under the auspices of the U.S. Department of Energy by Lawrence Livermore National Laboratory under Contract DE-AC52-07NA27344.